Diffusion Tensor Imaging Summary Measures in White Matter Regions of Interest

Talia M. Nir, Sophia I. Thomopoulos, Julio E. Villalón-Reina,
Neda Jahanshad, Paul M. Thompson

Imaging Genetics Center, Mark & Mary Stevens Neuroimaging & Informatics Institute,
Keck School of Medicine, University of Southern California, Marina del Rey, CA.

Summary

In ADNI2, diffusion-weighted MRI (dMRI) data were acquired with one acquisition protocol from approximately one third of enrolled participants at the subset of sites with General Electric (GE) scanners; in its third phase, ADNI3 has incorporated numerous new dMRI protocols for Siemens, Philips, and GE scanners to allow dMRI data collection at all sites (http://adni.loni.usc.edu/methods/documents/mri-protocols/). We have updated our dMRI preprocessing methods – that reduce common sources of noise and artifacts—to accommodate both the updated ADNI acquisition protocols and more recent advances in available tools. We compute four standard diffusion tensor imaging (DTI)[1] measures including fractional anisotropy (FA) and mean, radial, and axial diffusivity (MD, RD, AxD) from corrected dMRI images. Mean DTI measures are then extracted from 73 white matter (WM) regions of interest (ROIs) from the John Hopkins University (JHU) WM atlas.

Methods

Preprocessing steps

Raw dMRI data were first denoised with PCA-based algorithms[2] using DiPy[3]. For the data that had the original acquisition matrix (i.e., Siemens and Philips protocols), principal components were classified via the Marchenko-Pastur distribution of the eigenvalue spectrum (i.e., MP-PCA)[4, 5]. dMRI data that were zero-padded in k-space (i.e., GE protocols where data were zero-padded to 256 x 256 matrices[a]) principal components were classified based on the local variance of the image Rician noise distribution (i.e., LPCA)[2]. Denoised dMRI were then corrected for Gibbs ringing with MRtrix[6, 7], extra-cerebral tissue was removed using FSL's *bet*, and eddy correction performed using FSL's *eddy_cuda* tool[8] with *repol* outlier estimation and replacement[9] and *slice-to-volume* correction[10]. dMRI then underwent ANTs N4 B1 field inhomogeneity corrections[11].

Raw T1-weighted (T1w) images, masked with HD-BET[12], were preprocessed using the standard FreeSurfer pipeline[13] and linearly aligned to the MNI-ICBM52 T1w template. dMRI b_0 images were then linearly aligned to resulting T1w images with FSL's *flirt* boundary-based registration (BBR)[14], using respective FreeSurfer derived WM masks. The dMRI data were not acquired with opposing phase-encoding polarities which are necessary to correct echo-planar imaging (EPI) induced susceptibility artifacts with tools like FSL's *topup*. Instead, ANTs[15, 16] three-channel non-linear registration was used to warp each participant's dMRI to their respective T1w; DTI FA, MD, and

---

[a] Raw zero-padded GE scans have 0.9x0.9x2.0 mm³ voxel dimensions rather than 2x2x2 mm³
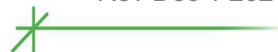
mean b_0 equally drove registrations to T1w images. The linear and non-linear registrations were concatenated and inverted; the resulting deformations were then applied to all unregistered dMRI volumes to both correct images for susceptibility-induced distortions and bring them back to their native space with only 1 interpolation. The distortion corrected dMRI were then run through FSL's *fast* bias field inhomogeneity correction[17] using MRtrix's *dwibiascorrection* wrapper.

DTI FA, MD, RD, and AxD scalar maps[1] were estimated from corrected data with FSL's *dtifit* using weighted least squares. For multi-shell acquisitions, DTI measures were estimated using only the subset of b_0 and b=1000 s/mm^2 DWI volumes.

White matter tract atlas ROI summary measures

The JHU ICBM-DTI-81 atlas FA map was warped to each participant's FA with ANTs[13] and the transformations applied to the stereotaxic WM atlas labels[18] (http://cmrm.med.jhmi.edu/cmrm/atlas/human_data/file/AtlasExplanation2.htm) using nearest neighbor interpolation. For each participant, the *mest* iterative M-estimator from the 'WRS2' package[19] in R (https://cran.r-project.org/web/packages/WRS2/index.html) was used to calculate a robust mean of FA, MD, RD, and AxD values within 73 WM ROIs (**Table 1**). For each ROI, the standard mean is also provided.

Dataset Information

This methods document applies to the following dataset(s) available from the ADNI repository:

Dataset Table Name	Method
USC - DTI ROI Summary Measures v2 (Mean)	Mean across ROI voxels
USC - DTI ROI Summary Measures v2 (Robust Mean)	Robust mean across ROI voxels
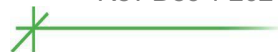
Table 1. Index of JHU WM atlas labels

ROI	Hemisphere	Notes:
Superior cerebellar peduncle	left, right, average	*check FOV
Inferior cerebellar peduncle	left, right, average	*check FOV
Middle cerebellar peduncle		*check FOV
Pontine crossing tract		a part of MCP, *check FOV
Medial lemniscus	left, right, average	*check FOV
Cerebral peduncle	left, right, average	*check FOV
Corticospinal tract	left, right, average	
Anterior limb of internal capsule	left, right, average	
Posterior limb of internal capsule	left, right, average	
Retrolenticular part of internal capsule	left, right, average	
Anterior corona radiata	left, right, average	
Superior corona radiata	left, right, average	
Posterior corona radiata	left, right, average	
Cingulum	left, right, average	cingulate gyrus
Cingulum (hippocampus)	left, right, average	
Fornix (cres) / Stria terminalis	left, right, average	cannot be resolved with current resolution
Superior longitudinal fasciculus	left, right, average	
Superior fronto-occipital fasciculus	left, right, average	could be a part of anterior internal capsule
Sagittal stratum	left, right, average	includes inferior longitudinal fasciculus and inferior fronto-occipital fasciculus
External capsule	left, right, average	
Uncinate fasciculus	left, right, average	
Posterior thalamic radiation	left, right, average	includes optic radiation
Tapetum	left, right, average	
Fornix		column and body of fornix
Genu of corpus callosum		
Body of corpus callosum		
Splenium of corpus callosum		
Full internal capsule		
Full corpus callosum		
Full corona radiata		
Full white matter		includes all ROIs

* Warning: DWI may have a cropped field of view (FOV) and reported means may not capture the full ROIs; these regions are also frequently subject to motion and artifact and may be less reliable

REFERENCES

1. Basser, P.J., et al., *MR diffusion tensor spectroscopy and imaging.* Biophys J, 1994. **66**(1): 259-67.
2. Manjon, J.V., et al., *Diffusion weighted image denoising using overcomplete local PCA.* PLoS One, 2013. **8**(9): e73021.
3. Garyfallidis, E., et al., *Dipy, a library for the analysis of diffusion MRI data.* Front Neuroinform, 2014. **8**: 8.
4. Veraart, J., et al., *Diffusion MRI noise mapping using random matrix theory.* Magn Reson Med, 2016. **76**(5): 1582-1593.
5. Veraart, J., et al., *Denoising of diffusion MRI using random matrix theory.* Neuroimage, 2016. **142**: 384-396.
6. Kellner, E., et al., *Gibbs-ringing artifact removal based on local subvoxel-shifts.* Magn Reson Med, 2016. **76**(5): 1574-1581.
7. Tournier, J.D., et al., *MRtrix3: A fast, flexible and open software framework for medical image processing and visualisation.* Neuroimage, 2019. **202**: 116137.
8. Andersson, J.L.R. and S.N. Sotiropoulos, *An integrated approach to correction for off-resonance effects and subject movement in diffusion MR imaging.* Neuroimage, 2016. **125**: 1063-1078.
9. Andersson, J.L.R., et al., *Incorporating outlier detection and replacement into a non-parametric framework for movement and distortion correction of diffusion MR images.* Neuroimage, 2016. **141**: 556-572.
10. Andersson, J.L.R., et al., *Towards a comprehensive framework for movement and distortion correction of diffusion MR images: Within volume movement.* Neuroimage, 2017. **152**: 450-466.
11. Tustison, N.J., et al., *N4ITK: improved N3 bias correction.* IEEE Trans Med Imaging, 2010. **29**(6): 1310-20.
12. Isensee, F., et al., *Automated brain extraction of multisequence MRI using artificial neural networks.* Hum Brain Mapp, 2019. **40**(17): 4952-4964.
13. Fischl, B., et al., *Automatically parcellating the human cerebral cortex.* Cereb Cortex, 2004. **14**(1): 11-22.
14. Greve, D.N. and B. Fischl, *Accurate and robust brain image alignment using boundary-based registration.* Neuroimage, 2009. **48**(1): 63-72.
15. Avants, B.B., et al., *Symmetric diffeomorphic image registration with cross-correlation: evaluating automated labeling of elderly and neurodegenerative brain.* Med Image Anal, 2008. **12**(1): 26-41.
16. Avants, B.B., et al., *A reproducible evaluation of ANTs similarity metric performance in brain image registration.* Neuroimage, 2011. **54**(3): 2033-44.
17. Zhang, Y., et al., *Segmentation of brain MR images through a hidden Markov random field model and the expectation-maximization algorithm.* IEEE Trans Med Imaging, 2001. **20**(1): 45-57.
18. Mori, S., et al., *Stereotaxic white matter atlas based on diffusion tensor imaging in an ICBM template.* Neuroimage, 2008. **40**(2): 570-582.
19. Mair, P. and R. Wilcox, *Robust statistical methods in R using the WRS2 package.* Behavior Research Methods, 2020. **52**(2): 464-488.